The complex atmospheric corrosion of α/δ bronze bells in a marine environment

A. Petitmangin, I. Guillot, A. Chabas, S. Nowak, M. Saheb, S.C. Alfaro, C. Blanc, C. Fourdrin, P. Ausset

The complex atmospheric corrosion of α/δ bronze bells in a marine environment.

A. Petitmangin*[(a)], I. Guillot [(b)], A. Chabas [(a)], S. Nowak[(c)], M. Saheb [(a)], S. C. Alfaro[(a)], C. Blanc[(a)], C. Fourdrin[(d)], P. Ausset[(a)].

(a) Univ Paris Est Creteil and Université de Paris, CNRS, LISA, F-94010 Créteil, France

(b) Université Paris Est (UPE), Institut de Chimie des Matériaux Paris-Est ICMPE-UMR 7182 CNRS-UPEC, 2 rue Henri Dunant, 94120 Thiais France

(c) UFR de Chimie-Université Paris Diderot, 35 rue Hélène Brion, 75205 Paris Cedex 13 France

(d) Laboratoire Géomatériaux et Environnement (EA 4508), UPEM, Université Paris-Est, 77454 Marne la Vallée cedex, France

Corresponding author: A. Petitmangin*
Tel: +33 1 82392052; E-mail address: aline.petitmangin@lisa.ipsl.fr

ivan.guillot@glvt-cnrs.fr (I. Guillot), anne.chabas@lisa.ipsl.fr (A. Chabas), sophie.nowak@univ-paris-diderot.fr (S. Nowak), mandana.saheb@lisa.ipsl.fr (M. Saheb), stephane.alfaro@lisa.ipsl.fr (S.C. Alfaro), caroline.blanc@lisa.ipsl.fr (C. Blanc), chloe.fourdrin@u-pem.fr (C. Fourdrin), patrick.ausset@lisa.ipsl.fr (P. Ausset).

Abstract:

α/δ bronze bells are heritage materials subject to corrosion. The alteration of a high-tin bronze bell casted in the 1930s and exposed to a marine environment in a steeple was studied. The ternary bronze (Cu-Sn-Pb) alloy displays inclusions and a porosity due to micro-shrinkages and poor gas evacuation. This altered bronze is characterized to (1) assess the influence of the manufacturing techniques and (2) hypothesize a micro-infiltration scenario of its alteration.

After exposure to the atmosphere, a transformed superficial medium overlaying layers of atacamite-paratacamite-cassiterite appears. Under them, the corrosion of the α dendritic structure and α/δ eutectoid characteristic of bronze bell is evidenced. The α pitting has a pronounced multilayered structure of cassiterite and cuprite-copper chloride, whereas the δ corrosion is composed of cassiterite and traces of cuprite. To understand better the lead impact on corrosion process, samples of the alloy were exposed in the laboratory to a synthetic marine solution.

The long-term corrosion behavior of the studied bell shows some similarities to those of other high tin bronze artefacts. The hypothesis of a corrosion scenario emphasizes the importance of the bells manufacturing techniques, α/δ structure of the ternary Cu-Sn-Pb alloy, and infiltrating networks of environmental fluids.

Keywords: α/δ bronze bells; Cu-Sn-Pb ternary alloy; atmospheric corrosion; micro-infiltrating alteration scenario.

1. Introduction

The bronzes undergo significant atmospheric alteration. The wet/dry cycles, resulting from the relative humidity and temperature fluctuations, the exposition to the atmospheric gases, most notably oxygen, combined with gaseous pollutants such as SO_2, O_3, NO_2 [1,2] as well as chloride aerosols in marine environments [3], are the prime factors responsible for bronze corrosion. To understand better the influence of atmospheric parameters, Cu-Sn alloys have been corroded by electrochemical techniques [4-5] or in alteration chambers [6]. Suitable conservation treatments for the traditional copper alloys [7] were proposed.

Atmospheric alteration can be regarded as a corrosion mechanism under the presence of an electrolyte film, caused by precipitations or water condensation at the metal surface. According to Robbiola's qualitative model [8], ionic migration through the alteration layer is common trait of all bronze corrosion processes: a layer of tin oxide rapidly forms and constitutes a diffusion barrier for the electrolyte film. Two mechanisms, controlled by aggressiveness environment can occur.

In the less corrosive environments, Type I corrosion is governed by the decuprification process: the cations from the alloy diffuse to the surface and control the rate of the alteration, which is generally slow. This leads to the formation of a compact layer of corrosion products, retaining the shape and volume of the object. The patina is formed of a tin-rich layer in contact with the alloy and passivates it. The outer layer consists of copper oxides with anions from the environment (formation of copper I or II minerals). In the Type II mechanism, which occurs in aggressive environments, an anionic control governs the corrosion and the corrosion rate is higher. A noticeable change in the volume and shape of the object is observed. Direct exposure to rainfall or not also makes a difference. In sheltered conditions, the anions precipitate with copper to form thick, more or less porous, corrosion strata overlaying a tin-rich layer. With rain, copper is washed out leading to a bronze dissolution. In these conditions, the corrosion layer is composed of soluble copper compounds and of tin oxide segregation more uniformly distributed in the depth of the patina.

In the type II mechanism, chlorine from marine atmosphere plays an active role. Active cyclic corrosion "bronze disease", based on a pitting process and relying on Lucey's membrane cell theory can take place [9, 10]. The layer of copper oxide-based corrosion products acts as a selective membrane allowing diffusion of chloride and oxygen ions towards the patina/alloy interface: O^{2-}, Cl^- inward and copper ions outward. Nantokite CuCl, precursor of copper hydroxy-chloride $Cu_2Cl(OH)_3$, develops and the $CuCl/Cu_2Cl(OH)_3$ transformation is facilitated by the patina porosity, allowing the penetration of humidity and oxygen. Due to a volume expansion, copper hydroxy-chlorides can deteriorate the object by flacking [11]. Regarding the tin of the alloy, even if it generally leads to better corrosion resistance, this behavior, not universal, depends on the chlorine content of the environment [12]. With little chlorine, the tin oxide, on contact with the alloy, improves the protective effect of the patina. But with high chlorine contents [13, 14] in marine atmosphere, tin oxide strata can develop throughout the patina thickness (sublayer of Cu_2O and $Cu_2Cl(OH)_3$ interposed by SnO_2 layers), making it less protective due to a strong dissolution of copper which approaches pure

copper. Redox reactions between intermediate products of tin and copper chlorides participate in the development of this stratification.

Most past studies of the bronze atmospheric corrosion focused on statuary and industrial bronzes of low tin content (<15 weight percent (%wt)), which are characterized by a predominant dendritic α-phase structure though they may also contain traces of δ-phase areas with higher tin content, under the form of (α+δ) eutectoid between the dendritic arms.

If the tin content is larger (15-27% wt), the relative importance of the (α + δ) eutectoid increases. In the case of hyper-eutectoid bronzes (tin content over 26% wt), fine δ dendrites are surrounded by the (α + δ) eutectoid [15, 16]. Independently of the tin content, ancient or modern bronze also often contains lead globules [15, 17, 18]. In the literature, the corrosion studies of the high tin bronzes are often focused on buried archeological bronzes (such as defensive weapons and decorative items, musical instruments) submitted to alteration conditions which are different from atmospheric corrosion (not the same humidification / drying cycles, nor the same nature and concentrations of potentially corrosive agents).

Bells are an important part of the heritage bronzes. Their alloys have a high tin content and a two-phase α/δ structure [19]. They are produced using ancient manufacturing methods combining the lost wax casting technique, commonly used in the past for the production of objects with a high tin content [16, 18] and the sand casting technique. Indeed, the mold of a bell, mainly made of clay, has 3 parts: the core (interior mold), the false bell, an intermediate mold on which are affixed wax inscriptions and the screed (outside mold). After heating, the wax melts and the false bell is separated from the screed and then destroyed. The volume left between the core and the screed, where the negative of the inscriptions rests in the interior, corresponds to the volume of the future cast bell. After unmolding, successive finishing techniques (deburring, sandblasting, final polishing) are used to polish the outside of the bell. Not being visible, the inside is left "foundry raw". The manufacturing techniques have evolved constantly since the Middle Ages to improve the fusion and the quality (lifespan and sound quality) of the cast bell. Being geographically widespread and exposed in steeples or outdoors, bells undergo corrosion representative of different anthropically-modified atmospheric environments. This feature makes of bells a good potential indicator of the territorial pollution [20]. Their oxide layers reflect the long-term physicochemical interactions between the metal substrate and the atmosphere, constituting a relevant imprint of the alloy's history. The bells are works of art with a high historic and symbolic value. They are musical instruments and belong to the material and non-material world heritage.

2. Research aim

Beside atmospheric corrosion, the bronze bell is submitted to shocks and vibrations generating the sound. This mechanical stress might affect the corrosion behavior. The impact of the α/δ alloy structure on its atmospheric corrosion still needs to be investigated, as the effect of its ternary composition (Cu-Sn-Pb) on the α and δ corrosion.

To document the impact of the particular microstructure of high-tin bronzes and of the atmospheric conditions on alteration, we characterize the corrosion of a bronze bell casted in the 1930s and exposed 90 years to a marine atmosphere in a steeple, shuttled from direct rain.

The composition and structure of the alloy and of the natural patina were studied and discussed in relation with the bell manufacturing techniques. To better understand the impact of the alloying elements on the corrosion, alloy samples were exposed in the laboratory to a synthetic electrolyte representative of marine environment. According to our samples, to understand better the corrosion behavior of the bronze bells, and to defend this tangible and intangible heritage, the corrosion behaviour of the bell is compared to the literature concerning the corrosion of different high tin bronze artefacts and the hypothesis of a micro-infiltrating alteration scenario is proposed.

3. Material and methods

3.1. Samples

Because ancient bells are often classified as World Heritage, exposed in museums, or/more simply worth of conservation, their sampling is limited and only performed on bells intended to the redesigned with the agreement of the bell-founders. Moreover, the brittle adhesion of the patina to the alloy sometimes makes the sampling difficult. So, the overall number of samples available for analysis remains limited and does not allow a statistical analysis of the corrosion layers. In this study, samples could be collected on a French bell, cast by the Cornille-Havard Company in 1930. The bell was exposed to a marine environment in the church of the coastal city of Trélévern in Brittany (France). It remained for about 90 years in a steeple, and was thus sheltered from direct rainfall. Cross-sections (1-3 cm^2) were taken from the crown and the profile, on the internal face of the bell where the mechanical stresses are the most important (action of the clapper, point of attachment of the crown). Therefore, this choice allows studying the impact on corrosion of the combination of mechanical and environmental constraints. Some samples were used for alloy characterization after chemical attack (alcoholic $FeCl_3$) and others for compositional analysis. Prior to the alloy and corrosion layer characterization, they were molded in resin and polished using SiC paper and diamond paste with ethanol to avoid any phase modification due to contact with water. For short corrosion tests in artificial marine solution, some samples of the alloy were polished with the same method.

3.2 Artificial marine solution

A synthetic solution representative of marine environment was prepared with analytical grade reagents and ultra-pure deionised water (Table 1):

	pH	**$[NO_3^-]$**	**$[Na^+]$**	**$[SO_4^{2-}]$**	**$[HCO_3^-]$**	**$[Cl^-]$**
Marine	5 - 6.35	1.55	4.97	3.11	0.24	13.10

Table 1: Composition ($g.mL^{-1}$) and pH of the marine solution used for the laboratory experiments.

Three 1 cm^2 alloy samples were immersed each in 50 ml of the solution for 3, 7, and 14 days. The temperature was maintained at 298K. The pH, (initially 5) increased slowly (Table 2), an obvious consequence of a corrosion process where the principal cathodic reaction is $O_2 + H_2O+2e^- \rightarrow 2OH^-$ [21].

Immersion times (days)	0	3	7	14
PH (± 0.01)	5.00	5.62	6.14	6.35

Table 2: pH measurements of the marine solution for the different immersion times.

3.3. Characterization

The ICP-OES analyses were made on two cubic samples (8 mm^3) from the crown and the profile of the bell alloy (Varian VistaPro). For each test, 50 to 70 mg of alloy were mineralized into aqua regia (0.75 mL of HNO_3 and 2.25 mL of HCl) in a PTFE bomb placed in an oven at 80°C for 4h. The solutions with high concentrations in any given element (>1%wt) were diluted, while low concentration ones (<1%wt) were analyzed directly. For each element, measurements were performed three times at three different wavelengths to assess the reproducibility of the results.

The patina composition was observed in cross sections by SEM with MERLIN and JEOL JSM6301F microscopes (accelerating voltage: 15 keV and 8 keV) and analyzed by EDS (SSD detector). The samples were covered by a platinum conductive layer beforehand.

The identification of crystalline phases was performed using X-ray microdiffraction in zones of the patina selected after SEM observations. The equipment was a Panalytical Empyrean diffractometer in the Bragg-Brentano θ-θ configuration, using a Cu radiation ($\lambda_{K\alpha}$=1.541874 Å). The maximum analyzed area of the sample (at low angle) was 0.25 mm^2. Each pattern was recorded in the 15°-80° range.

Raman microspectrometry was also used to identify the corrosion products. Measurements were carried out with a Renishaw In Via spectrometer with a 100x optical microscope LEICA objective. The laser spot was less than 1 µm in size and the laser power was filtered down to 0.25mW, avoiding the thermal modification of the corrosion products. The excitation wavelength of 532 nm was used and the spectra acquisitions were managed at a resolution of 1.7 cm^{-1}.

4. Results

4.1. Bronze substrate

The alloy composition, obtained by ICP-OES for different areas of the crown and profile, highlighted no significant difference between the sampling zones. Thus, the average composition of the samples (Table 3) can be assumed to be the overall composition of the bell.

	Cu	Sn	Pb	Sb	Zn	As	Ni	S	Fe
Weight percent (wt %)	77.3±1.1	21.82±0.12	1.22±0.01	0.18±0.01	0.26±0.01	0.16±0.01	0.05±0.01	0.04±0.01	0.01±0.01

Table 3: Average chemical composition (wt %) of the bell.

The bell has a tin content of about 22 wt%. A particularly high lead content (1.22 wt%) and some impurities are evidenced. These particularities will be further discussed (§5).

Optical microscopic observations (Fig.1a) confirm the two-phase microstructure of the alloy: a dendritic α single phase with an eutectoid α/δ interspersed between the dendritic arms. δ has a higher tin content (Sn 31.84%wt) than α (Sn 14.94%wt) (Fig. 1b), in agreement with the Cu-Sn phase diagram [19].

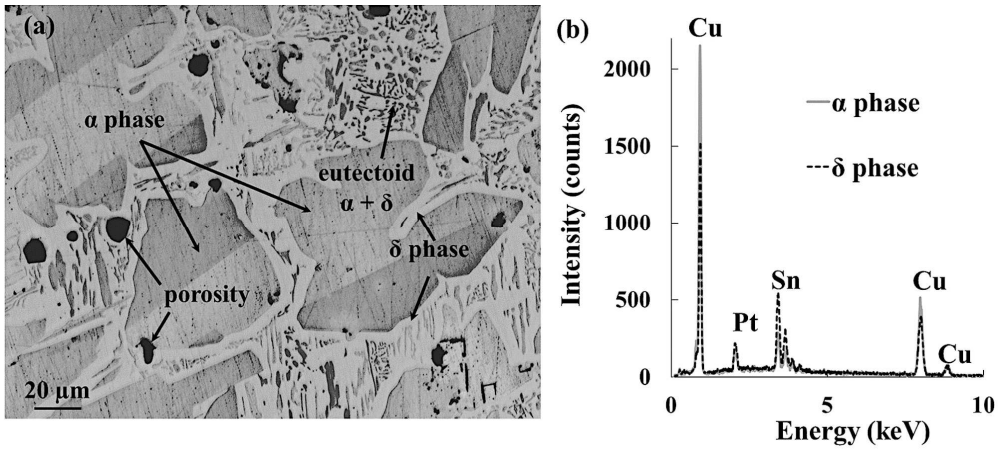

Fig. 1: (a) Optical micrography of the microstructure of the internal part of the bell. In the α/δ eutectoid, the δ phase appears in lighter shade of gray and α in gray. (b) EDS analyses of α and δ phases.

Microscopic observations reveal in interdendritic spaces some porosities, which are due to micro-shrinkages or to a large content of gas in the liquid metal during the casting. Some of the cavities could possibly be ascribed to lead globules being removed during the sample preparation. SEM-EDS observations reveal some residual crystals, corresponding to lead and lead oxides (Fig. 2). Because of the insolubility of lead in the bronze matrix [22], the alloy can be considered as a ternary bronze Cu-Sn-Pb (Pb 1.22%wt-Table 3).

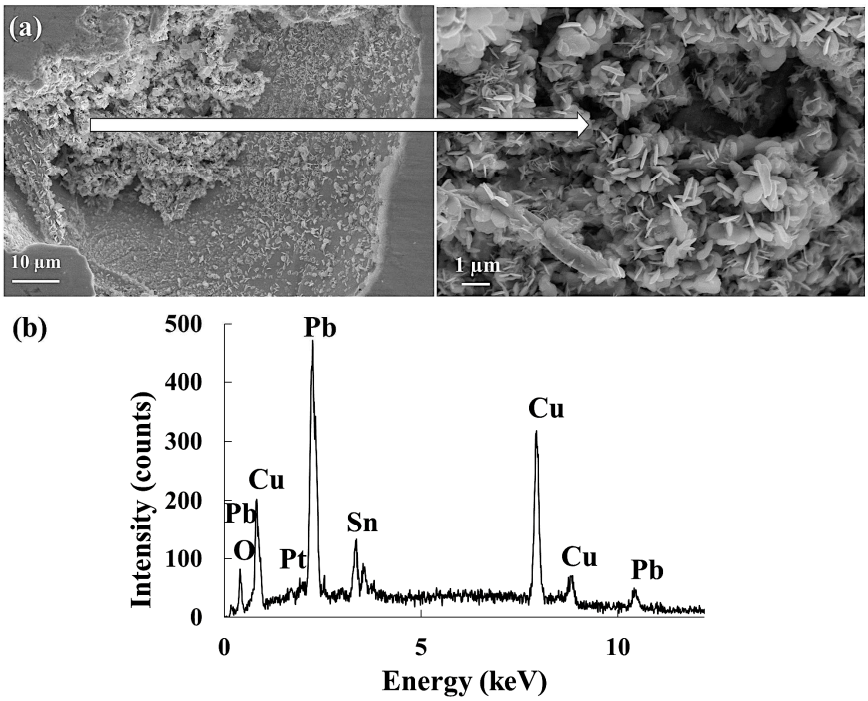

Fig.2: (a) SEM-BSE image and (b) SEM-EDS analyses of alloy porosities.

4.2. Characterization of the patina

To understand better the corrosion, SEM-EDS and micro XRD analyses were performed on cross sections of the internal face of the bell (Fig.3). The choice of a specific sampling zone (crown or profile) did not affect the structure and composition of the corrosion. The SEM observations highlighted three distinct alteration areas: **(i)** A porous **external layer** presenting phases or elements characteristic of the bell mold. This layer corresponds to the transformed medium. **(ii)** A more or less continuous, **intermediate layer**. **(iii) Internal corrosion pitting** which mainly affects the α phase.

The patina is a fragile system and naturally micro-cracked, because of the chocks and vibrations induced by the clapper action. But, it is not possible to distinguish these pre-existing micro-cracks from those which could result from the collection of the samples on the "bell object".

4.2.1 The external layer

The external layer (Fig.3) is in localized zones, highly enriched in oxygen associated with silicon and iron and as compared to the intermediate layer, often depleted in copper and tin. The exogenous compounds are characteristic of an enrichment in clay, typical of the manufacturing techniques. Traces of lead are also observed and terrigenous or anthropogenic deposits can be associated with the exogenous compounds.

4.2.2 The intermediate layer

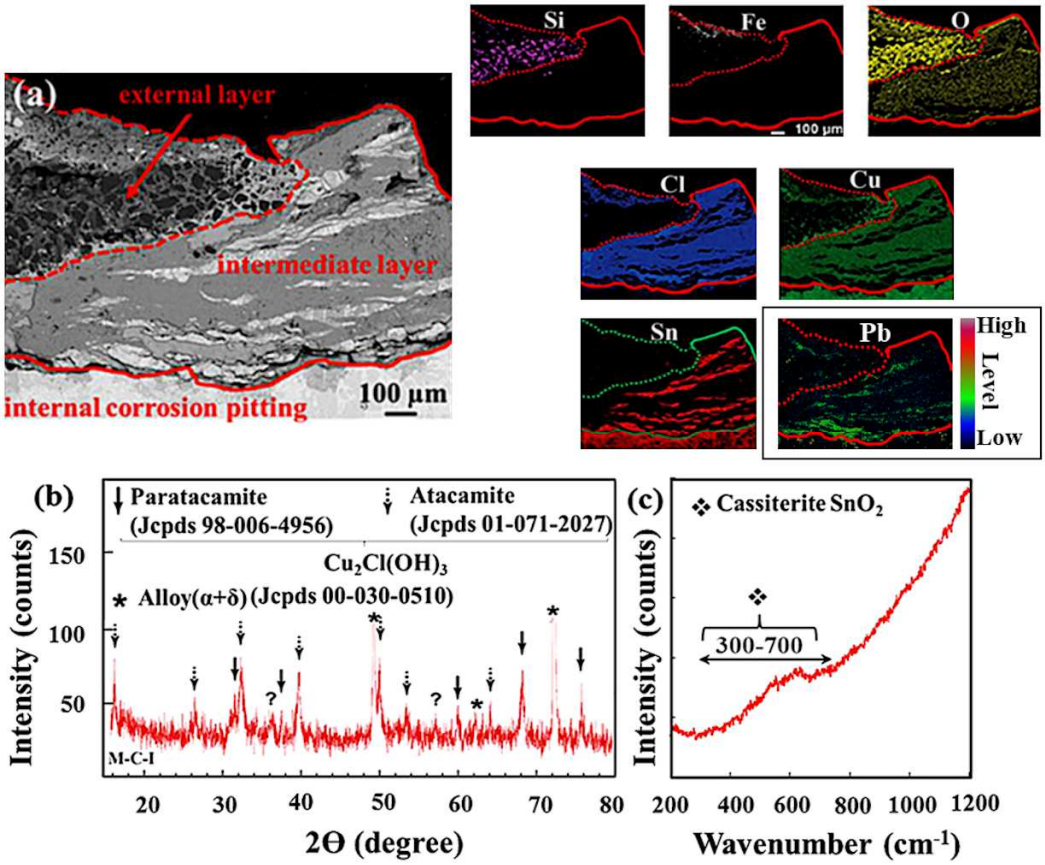

Fig. 3: The internal face of the bell crown: (a) SEM-EDS elements map with the level map of lead (b) Micro XRD analyses of the cross section (c) Raman analyses of the tin oxide.

On the internal part of the crown (Fig.3 (a)), a homogeneous EDS signal of oxygen in the intermediate layer is observed. The layer presents, thick zones enriched in both copper and chlorine alternating with, occasionally, as observed on Fig.3 (a), tin-enriched and copper depleted zones where lead is also present. The micro XRD patterns (Fig.3 (b)) of the same zones display mostly copper hydroxi-chloride compounds under atacamite and paratacamite ($Cu_2Cl(OH)_3$) and a lack of tin species. This lack could be imputed to the amorphous nature of tin oxide [4] or to the thickness of the areas, with large copper areas masking the XRD signal of the thinner tin zones. However, the broad band between 300 cm^{-1} and 700 cm^{-1} on the Raman analyses (Fig.3 (c)) is in support of the presence of nanometric crystallites of cassiterite SnO_2 [4,23]. No lead compounds were detected by Raman analyses certainly because of the low amount of this element in the tin corrosion products.

4.2.3 The internal corrosion pitting

Internal corrosion patterns of the α/δ alloy are observed under the intermediate corrosion layer. They are micro-cracked and divided into two parts: **(i)** The residual corroded primary α phase **(ii)** The α/δ eutectoid with the remains of the corroded δ phase. The internal corrosion pitting (Fig 3) shows also some more or less corroded lead globules.

a. Corrosion of the primary α phase

On the internal face of the crown (Fig.4) the oxygen EDS signal is sharp and uniformly distributed, characteristic of a strong corrosion. Oxygen is associated with chlorine and copper, with some areas of exception where these two elements are replaced by tin. The corrosion of α has a multilayer microstructure. Lead is also present in α dendrite corrosion. Its EDS signal is not located as lead corroded globules (Fig 3), but is associated with the tin signal, more characteristic of a diffusing behaviour in tin corrosion products. The Raman spectrum of the copper oxychloride layers (Fig 4 (c)) contains Cu_2O vibrations bands (148 and 220 cm^{-1} and a vibrational triplet at 420, 520 and 625 cm^{-1}). The thin layers, rich in tin compounds, show a weak band between 300 and 700 cm^{-1} more in agreement with the presence of SnO_2 [23], but Cu_2O traces are confirmed by the weak band near 220 cm^{-1}. No signal for copper chloride is present because of an amorphous behavior and no lead compounds, due to certainly their small quantity.

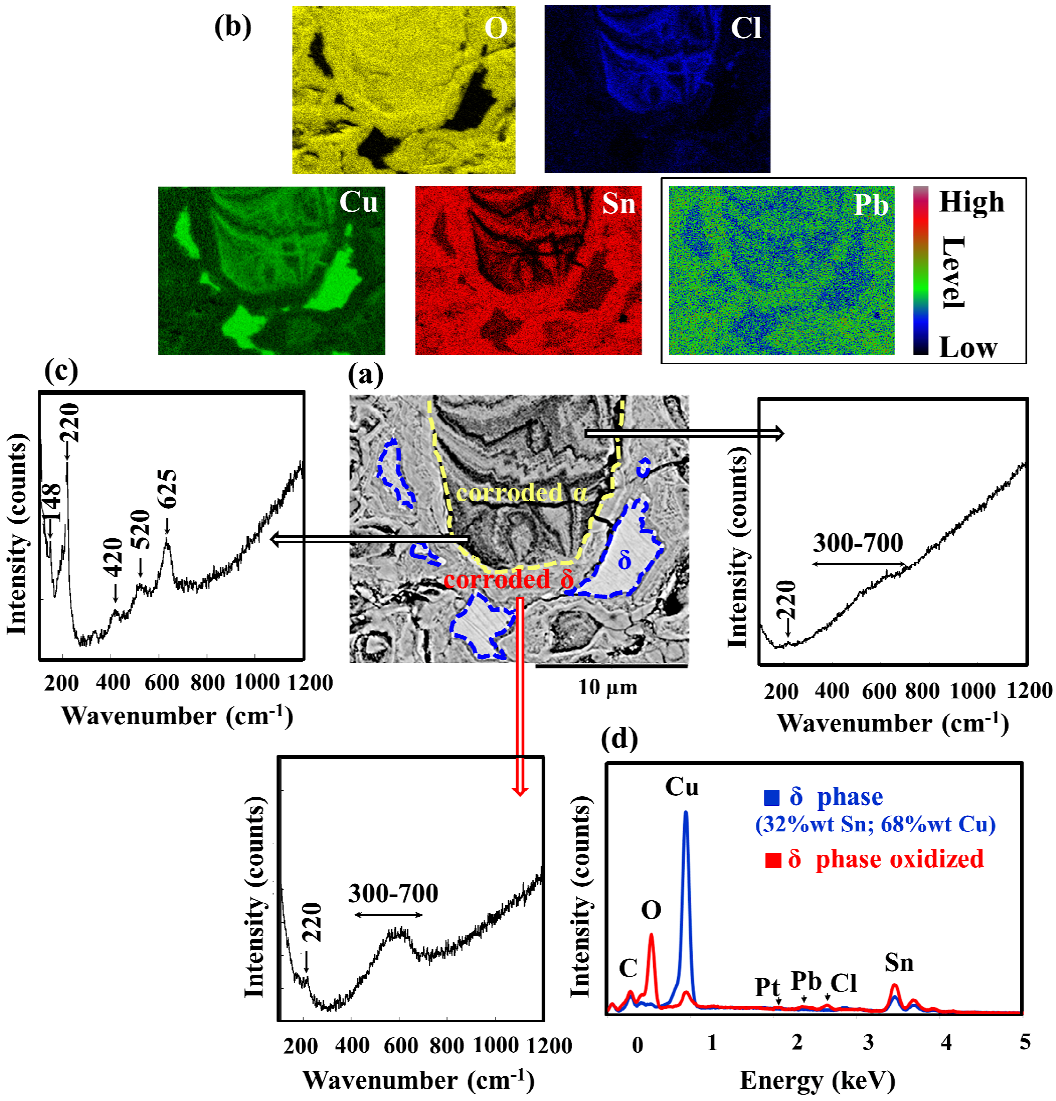

Fig. 4: On the SEM image (a), the corroded α phase is surrounded by yellow dotted lines and the δ phase by blue dots. Oxidized δ is in gray between them. (b) SEM-EDS map of Cu, Sn, O, Cl with the level map of Pb (c) Raman spectra of the corroded α phase and δ phase. (d) EDS analyses of the δ phase and the corroded δ phase.

b. Corrosion of the eutectoid

The eutectoid corrosion relates not only to the α phase but also to the δ one. On Fig.4, according to semi quantitative SEM-EDS analyses, the uncorroded δ phase is associated to the altered δ phase. No signal related to copper and chlorine, but a high concentration of tin with oxygen and little EDS signal of copper are detected in the corroded δ phase. This is due to an important copper depletion. The large band between 300 cm^{-1} and 700 cm^{-1} on the Raman analyses corresponds to a predominance of SnO_2 [23] and the very weak band at 220 cm^{-1} to Cu_2O, present in small quantity. Small amount of lead is also associated with tin EDS signal in altered δ phase.

4.3. Short corrosion of alloy specimens: the role of alloying elements

To study more specifically the role of lead on the corrosion of the α phase and the δ phase in the internal corrosion part of the old patina, uncorroded alloy specimens were immersed after 3, 7 and 14 days in a marine solution. To promote wetting time, and then the action of the electrolyte, we have chosen to favor continuous immersion.

Visual investigation of the alloy specimens reveals the progressive formation of a whitish grey area. The more or less porous surface of the alloy displays an irregular layer of corrosion products particularly rich in lead, oxygen and carbon, with chlorine traces (Fig. 5a). SEM observations (Fig. 5b) show hexagonal crystals in platelets. After 7 days, some prismatic crystals with an engraving of their edges are observed. Over these two forms of crystallites, the growth of small square-based crystals is observed.

The Raman analyses (Fig. 5c) show that the lead compounds are essentially carbonates. Indeed, the vibration band at 3550 cm^{-1} and that at 410 cm^{-1} , which is observed after 3 days and gradually disappears for longer exposures, correspond to hydrocerussite ($Pb_3(CO_3)_2(OH)_2$) [24]. This lead carbonate grows to hexagonal form [25, 26] as shown on the SEM images. The vibration band at 1053 cm^{-1} can be due to either hydrocerussite or cerussite (Pb_3CO_3) whose presence is confirmed by the observation of prismatic crystals (Fig. 5b) [24,27]. Lead sulfate is also present after 3 days of alteration, as indicated by the band near 960 cm^{-1}[28]. Moreover, the traces of chlorine on the EDS signal associated to the width of the band at 1053 cm^{-1}, particularly large after 14 days, reflect the presence of lead chloride in small quantity. Independently of the corrosion duration, there is always a small band at 185 cm^{-1} indicative of the presence of phosgenite ($Pb_2Cl_2CO_3$) [24]. These lead chlorides could correspond to the small square-based crystals observed on the SEM images. However, the presence of lead oxides cannot be excluded because of the square form of these crystallites [27,29]. After 14 days of alteration a large band is also observed, between 400 and 750 nm, corresponding to traces of copper oxide and a predominance of tin oxide [23].

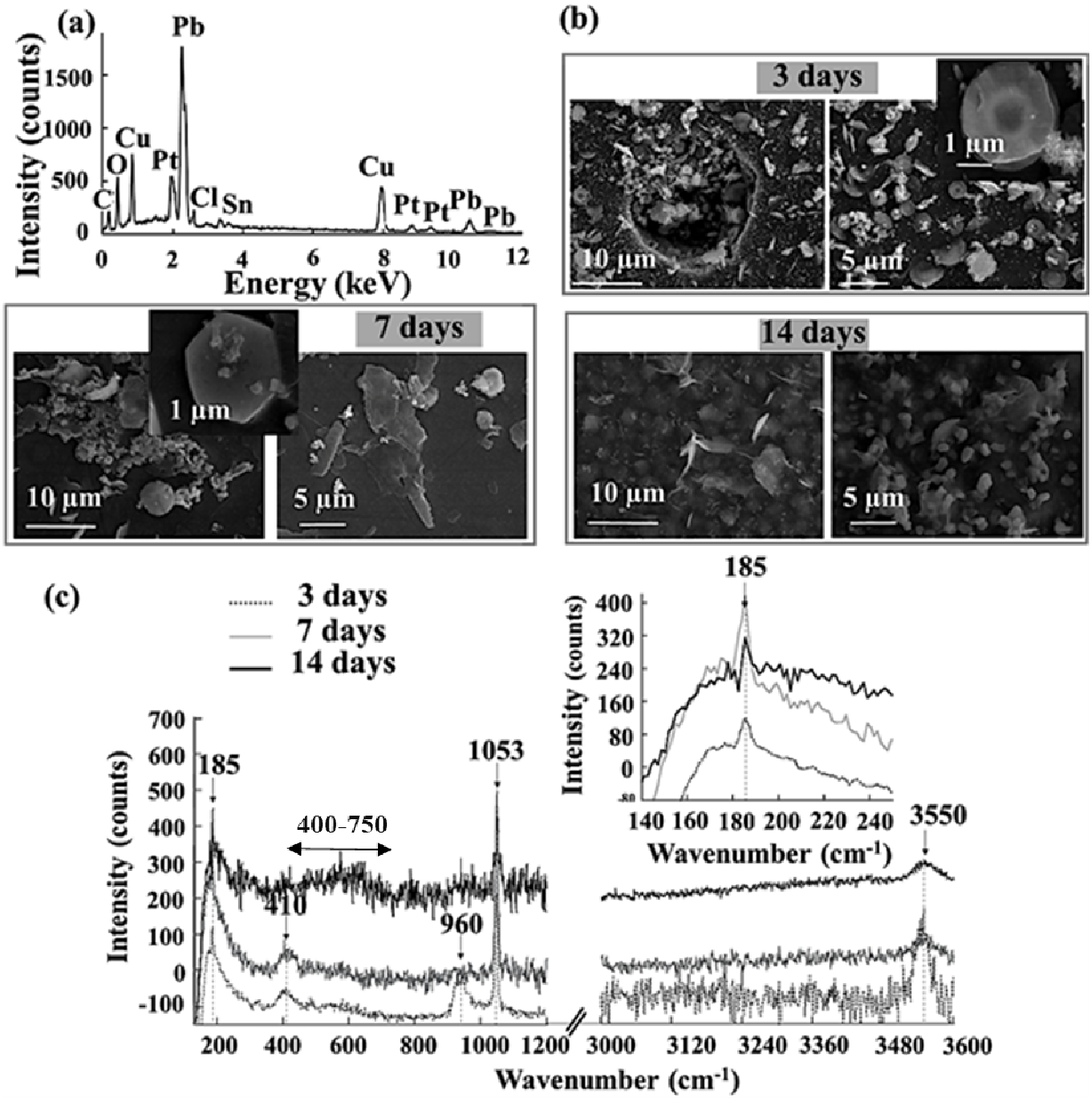

Fig.5: (a) EDS analysis and (b) SEM-BSE images for 3, 7 and 14 days of corrosion in marine solution. (c) Raman analysis of corrosion products.

The alloy microstructure (Fig 6) shows that, the lead corrosion pitting mainly develops on the dendritic and eutectoid α phase, whereas the δ phase which has a higher tin content presents less located lead and oxygen EDS signal. Whatever the duration of alteration, the same observations were made. However, after 14 days, some α dendrites display small octahedral crystals of cuprite as evidenced by the 218 cm^{-1} vibration band and the vibrational triplet (422 cm^{-1}; 525 cm^{-1}; 623 cm^{-1}) on the Raman spectra [23]. Trace of nantokite (CuCl) cannot be excluded as indicated by the thin band at 1065 cm^{-1} [30]. The role of Pb on the corrosion of Cu-rich dendrites and α/δ eutectoid will be discussed (§5).

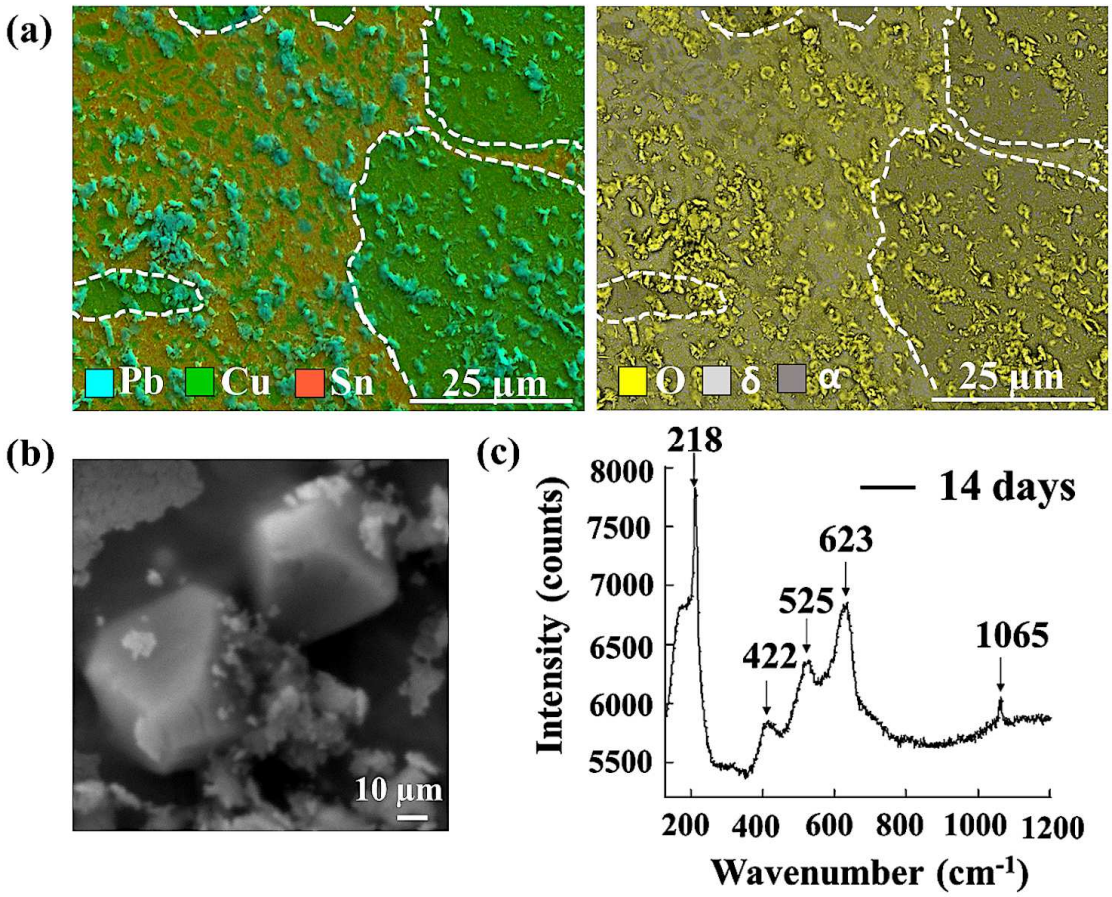

Fig.6: (a) SEM image of the alloy microstructure with Pb,Cu,Sn,O EDS signals for 3 days alteration. Dendritic α phase is surrounded by white dotted lines (b) SEM-BSE image of the Cu_2O octahedra and (c) their Raman spectrum (14 days of alteration).

5. Discussion:

5.1. The bells quality – the impact of manufacturing techniques

The bell from Cornille-Havard foundry, has a α/δ structure and a tin mass content (about 22 wt%-Table 3) corresponding to the theoretical composition of bronze bells, estimated by the technical Roret manual of 1827 [31] to be about equal to a quarter of the total mass when mixing pure metals. With this tin content, a sufficient amount of δ phase is formed which, by improving the bronze hardness [32], brings resonance to the instrument. However, the level of lead is not insignificant (1.2%wt). In the copper-lead system, all the α copper phase will solidify before the lead-copper eutectoid [19, 33, 34]. It will cause the formation of insoluble globules of Pb in the microstructure (Fig. 2) which makes of our alloy a ternary bronze (Cu-Sn-Pb). The lead in the alloy improves the fluidity of the melt and facilitates the machinability [16]. The finishing of the solidified castings is easier. Regarding the impurities in the alloy, they can come from the ores or from the use of recycled copper alloys by the bell-founders.

The bell alloy has a similar microstructure and composition to many archaeological bronzes with a high tin content (dishes, weapons or musical instruments). However, due to their regular use in ancient daily life, limiting the δ phase, responsible of the alloy fragility

was necessary. Thus, the tin content during casting of some bronze objects was often limited (10% wt to 18% wt) with a higher lead content, more closer to very hold bronze bells dating from the Middle Ages or the Empire [35, 36], with a greater proportion of α phase and lead inclusions. To facilitate their shaping, some ancient bronzes were also submitted to thermal and mechanical treatments, modifying their α/δ microstructure. Gongs or cymbals or other high tin bronze objects [37-39], made by hot forging and quenching, develop α grains in a martensitic ß or ɣ matrix, depending on their quenching temperature.

Finally, the manufacturing techniques of the bell affect the composition of the corrosion products. For instance, clay is used to make the heat resistant molds [31]. The clay exogenous elements subsequently combine with corrosion products to form a transformed medium on the external part of the corrosion. Moreover, the lead content of the alloy affects the corrosion: lead carbonates and chloride are present before the development of copper corrosion products.

5.2. Corrosion of the archaeological high-tin bronzes and the bell from Cornille-Havard foundry

A comparison, between the literature about the alteration of buried archaeological bronzes with high tin content and the atmospheric corrosion of the bronze bell studied, is necessary. According to our samples, the bell alteration has:

- Common points:

1/ Three distinct alteration areas (Fig.3): (i) a transformed medium on the extreme surface with exogenous elements and copper corrosion products but no transparent compact film rich in tin oxide, resulting from tinning (ii) an intermediate layer rich in environmental anions (iii) a preferential α/δ corrosion pitting in the underlying alloy (Fig.4) [15,18,40-42].

2/ A periodic corrosion of the α phase, resembling the liesegang phenomenon on buried archaeological bronzes [43] and associated with the Cu/Sn variations during the corrosion progression due to environment variations.

- Differences:

1/ No extend of inter-granular corrosion, due to impurities along the grain boundaries of the alloy, induced by mechanical and thermal treatment of some bronzes [44].

2/ No redeposition of metallic copper, often observed in bronze artefacts with high tin content [45-48]. This slow process takes place with low concentration of O [45,46] and reducing conditions. There are three classifications of copper redeposition [46]: (i) Related to long-term corrosion processes, irregular form pseudomorphically replacing other phases, due to a destannification, similar to the dezincification process, or a replace of corroded lead globules (in leaded bronzes) or cuprite in micro-cracks. (ii) During the casting, a twinned microstructure, because of incomplete mixing of copper and tin or (iii) a globular form during roasting of the copper ores.

3 / No preferential corrosion of δ associated with α phase remaining intact, observed with low oxygen potential and copper redeposition in bronze artefacts [48].

Finally, the patina of the internal face of our bell results from atmospheric gases, chloride aerosols and a slow wetting and drying of the condensation water which occurs due

to a roughness of the surface left "foundry raw". The difference with buried high tin bronzes is based on the oxygen concentration in the environment. Atmospheric conditions, lead to a preferential corrosion of the α phase and passivation of the δ phase, richer in tin. In poorly ventilated environments of certain soils, preferential corrosion of the δ with redeposition of metallic copper is observed, the α phase remaining intact. The properties variations of soil can cause higher O potential, leading to local structures typical of atmospheric corrosion in the same buried object [48] which highlights the oxygen impact on the α/δ preferential corrosion.

5.3. Hypothesis of an alteration scenario

In the case of our samples taken from a bell exposed in a marine environment for 90 years but, sheltered from direct rain in a steeple, an uniform enrichment in tin of the patina, in direct contact with the alloy, could have been expected, suggesting a type I corrosion mechanism, governed by a cationic control [8]. Conversely, atacamite/paratacamite, characteristic of an advanced bronze disease, but also a preferential corrosion by pitting of the α or δ phases were observed with an important penetration of environmental anions in the α phase, which suggest a more aggressive corrosion of type II. Moreover, the intermediate layer of the patina reveals thin discontinuous layers of different compositions (copper hydroxi-chlorides and occasionally tin oxide).

To explain this organization of the patina on a bronze bell, the corrosion scenario must not only take into account the environmental aggressiveness [8], but also the effect on the brittle corrosion products of shocks and vibrations submitted by the bell to ring. They lead to micro/nano-metric scale infiltrating networks into which the environmental fluids and humidity can penetrate.

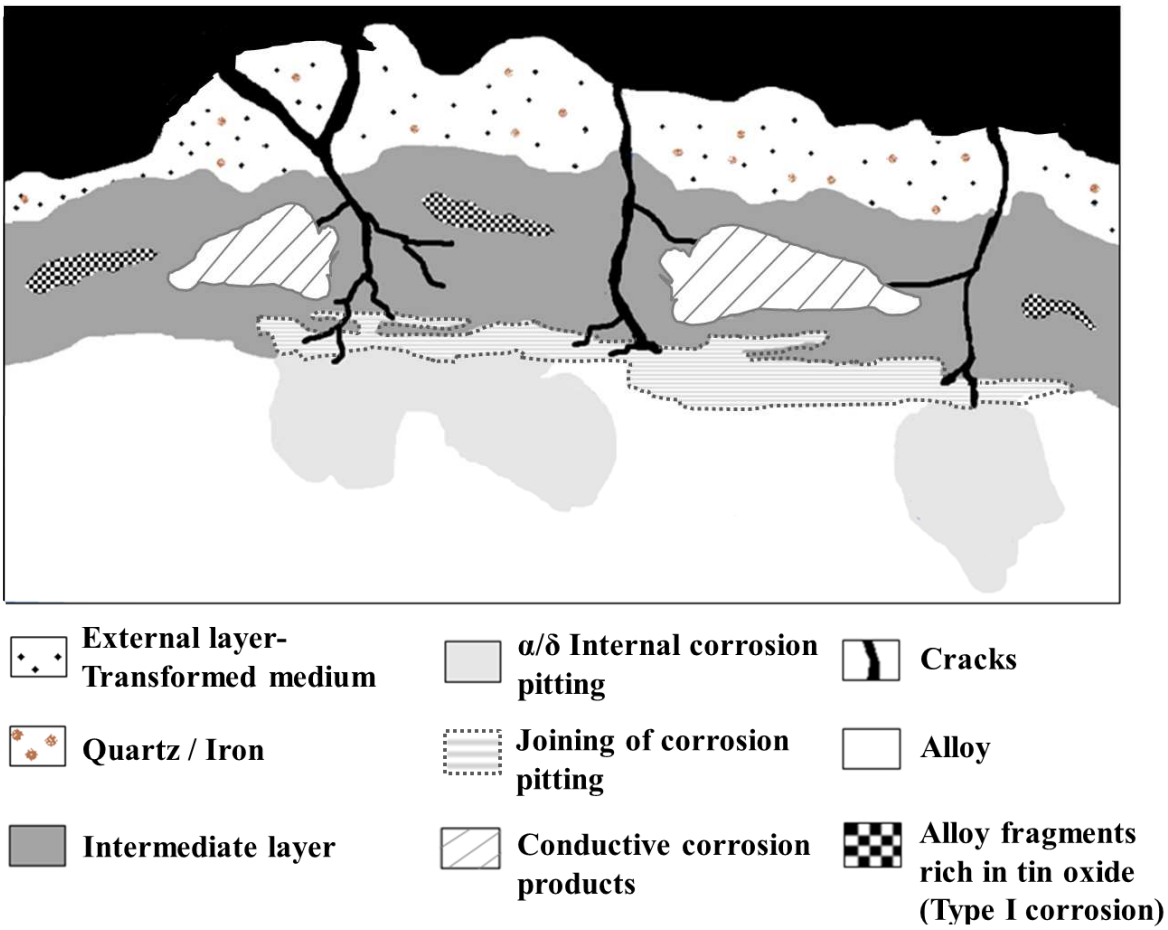

Fig. 7: Schematic representation of corrosion layers on the bronze bell: the development of internal corrosion pitting is favored by the micro-cracks inside the brittle patina and the interconnection of these pitting and the development of conductive corrosion products.

When environmental species and humidity migrate in contact with the underlying ternary (Cu-Sn-Pb) alloy, an electrochemical point of view is necessary. A galvanic corrosion can take place when dissimilar metals with different electrochemical potentials are electrically connected in an electrolyte [49]. Lead, being a less noble metal than copper and tin, acts as the anode. Pb serves as the primary electron donor and can be oxidized to Pb^{2+}. Excessive lead release caused by galvanic corrosion, with respect to copper, has been evidenced both in laboratory and field studies [50-53]. The galvanic corrosion between Pb and Cu is easier than between Pb and Sn because of a more important differential electrochemical potential. Because the corroded products of lead are unstable and soluble, they diffuse and migrate outwards through the alloy porosities and the infiltrating network. Near the empty cluster of lead, copper ions oxidize and deposit within the void of the lead globules. The Pb ions are replaced by redeposited Cu metal which in turn oxidizes to Cu giving the progression $Pb \rightarrow Cu \rightarrow Cu_2O$ [54] or $Pb \rightarrow Cu_2O \rightarrow Cu$ [16]. According to our results in laboratory, a pitting corrosion rich in lead carbonate develops mainly on the α dendritic and the α eutectoid phase, following the diffusion of Pb^{2+} ions on the surface. For δ, it does not present lead carbonates, or very little. This difference between the α and δ phases could be due to the higher tin content of the δ phase. Tin stabilizes as tin oxide, forming a passivation layer which is stable

over a wide range of pH and replaces the original alloy [8,55]. After a dissolution of lead carbonate, octahedral Cu_2O crystals on some areas of α phase was observed. It would support more a Pb → Cu_2O progression than Pb → Cu one. But these processes require additional investigations to be completely understood.

After this galvanic Cu-Pb corrosion phase, studied here in the laboratory, but which can occur under the natural patina of the bell when the corrosive agents migrate through the patina, the pitting corrosion of the α and δ phases takes place.

The corroded α phase exhibits a multi-layered system of tin oxide and copper oxy-chloride. Due to a good miscibility between lead and tin, as observed in the internal corrosion and the internal layer of the patina, Pb^{2+}, released by the galvanic corrosion migrate preferentially associated with tin corrosion products (Fig 3 et 4).

The alternating layers observed in the corroded α phase can be explained by comparing the thermodynamic stability of the copper and tin corrosion products: copper and tin are more stable when combined with oxygen than with chloride (Table 4) [56].

	SnO_2	**$SnCl_2$**	**Cu_2O**	**CuCl**
$\Delta H_g°$ (kJ.mol^{-1})	-515.8	-286.1	-146	-119.9

Table 4: Variation of standard free enthalpy ($\Delta H_g°$) for cassiterite (SnO_2), cuprite (Cu_2O), copper and tin chlorides.

These different stabilities contribute to the preferential growth of Cu_2O alternating with SnO_2, as evidenced by the Raman analysis. Regarding CuCl, it reacts easily with water and oxygen to form $Cu_2Cl(OH)_3$ [57,11] which is in low quantity and/or under amorphous form in the alternating Cu_2O enriched layers.

For the corrosion of the δ phase, only oxides are observed with majority of SnO_2 (Fig.4) and residual areas of uncorroded δ phase. The absence of a higher corrosion of δ phase with alternating layers as the α phase can be due to the stabilization of chlorine into the corrosion products of α, which slows down its migration into the internal areas of the eutectoid. The tin content in the δ phase, corroded and non-corroded, can also contribute to hinder the spreading of environmental species: the higher the alloy tin content, the more protective the patina is [55].

The more cracked the alteration layer is, the more permeable the patina becomes to the environment species (Fig.7). Thus, corrosion pits gradually tend to join together and the repetition of these reunions eventually favors the development of the intermediate layer.

In some areas of the intermediate layer, the alloy fragments detached from the metal matrix and present as inclusions in the patina induce a type I macroscopic behavior, with a strong decuprification of the fragments and a local enrichment in tin oxide (Fig.3 (a)). These islets of tin oxide in the depth of the patina (Fig.7) modify locally its protective influence.

If the conducting corrosion products (Fig.7) are present in the patina and are connected to the alloy, they transport electrons and provoke the decoupling of the anodic (bronze

corrosion) and cathodic (oxidant reduction) reactions. The first reaction occurs at the interface between the metal and the alteration layer. The second one occurs inside the corrosion layer or at its outer surface if the conductive phases are connected to the surface of the alloy. If these conducting oxides are not located near cracks or pores, traditional electrochemical alteration processes take place. Conversely, if the conducting oxide phases are adjacent to cracks, corrosion pits can develop around these cracks and eventually join to form a continuous layer throughout the patina.

Finally, as mentioned in the introduction [14], in marine atmosphere with high Cl^- and on bronzes with a low tin content, a multi-layer $Cu_2O/SnO_2/Cu_2Cl(OH)_3$ system has the particularity to be regularly distributed throughout the entire thickness of the patina, due to a lack of protection of SnO_2, which would lead to an increase in bronze disease. In our samples, due to the onset of type I corrosion of some alloy fragments incorporated into the patina, the tin oxide is observed in small quantity and more occasionally. But, this regular multilayer system seems to develop more in depth, under the micro-cracked patina, with α phase multilayered corrosion, while, the corroded δ phase is rich in SnO_2. This different α/δ behavior can be due to a higher δ tin content, making more efficient the passivity of SnO_2 on δ. Thus, with high Cl^- concentration in atmosphere, the accentuation of bronze disease due to SnO_2 doesn't seem to be universal and a limit value of the alloy tin content could reduce the atmospheric corrosion rate, but not prevent alteration. According to our results, it could be around the Sn content of the uncorroded δ phase, but more investigations are necessary to identify a possible tin limit value.

6. Conclusion

The corrosion of a high tin bronze bell, sheltered from direct rainfall in a steeple, but exposed for 90 years to a marine environment has been studied.

The micro-cracked patina is divided in an "external layer", with exogenous elements characteristic of bell foundry techniques, and an "intermediate layer" of atacamite, paratacamite, and some tin oxide. In bronze bell, "internal corrosion pitting" is highlighted. The α phase has a layered regular structure (cassiterite-cuprite, combined with cuprite-amorphous copper chloride bands). Tin oxide is the preferential product of the δ phase corrosion because of the large natural tin content of this phase, and chlorine stabilization in the corrosion products of the α phase. The atmospheric corrosion of the bell is quite similar to some buried high-tin bronze artefacts in sufficient aerobic conditions.

The hypothesis of the corrosion scenario emphasizes the bells manufacturing techniques, α/δ structure of the Cu-Sn-Pb alloy, and infiltrating networks.

Acknowledgements

This study is part of the BellACorr project supported by the French "Agence Nationale de la Recherche" (Project-ANR-18-CE27-0006).

Data Availability

The raw/processed data required to reproduce these findings cannot be shared at this time as the data also forms part of an ongoing study.

References

[1] S. Oesch, M. Faller, Environmental effects on materials: the effect of the air pollutants SO_2, NO_2, NO and O_3 on the corrosion of copper, zinc and aluminium. A short literature survey and results of laboratory exposures, Corros. Sci. 39 (1997) 1505-1530, https://doi.org/10.1016/S0010-938X(97)00047-4

[2] D.A. Scott, Copper and Bronze in Art: corrosion, colorants, conservation, in Getty Conservation Institute, Los Angeles (2002)

[3] N. Souissi, E. Sidot, L. Bousselmi, E. Trikki, L. Robbiola, Corrosion behaviour of Cu-10Sn bronze in aerated NaCl aqueous media - Electrochemical investigation, Corros. Sci. 49 (2007) 3333-3347, https://doi.org/10.1016/j.corsci.2007.01.013

[4] J. Muller, PhD Thesis, University of Paris-Est Creteil, France (2010), https://tel.archives-ouvertes.fr/tel-00492692/fr

[5] C. Chiavari, K. Rahmouni, H. Takenouti, S. Joiret, P. Vermaut, L. Robbiola, Composition and electrochemical properties of natural patinas of outdoor bronze monuments, Electrochim. Acta 52 (2007) 7760-7769, https://doi.org/10.1016/j.electacta.2006.12.053

[6] A. Chabas, A. Fouqueau, M. Attoui, S.C. Alfaro, A. Petitmangin, A. Bouilloux, M. Saheb, A. Coman, T. Lombardo, N. Grand, P. Zapf, R. Berardo, M. Duranton, R. Durand-Jolibois, M. Jerome, E. Pangui, J.J. Correia, I. Guillot, S. Nowak, Characterization of CIME, an experimental Chamber for simulating Interaction between Material of cultural heritage and Environment, Environ. Sci. Pollut. Res. 22 (2015) 19170-19183, https://doi.org/10.1007/s11356-015-5083-5

[7] M. Albini, P. Letardi, L. Mathys, L. Brambilla, J. Schröter, P. Junier, E. Joseph, Comparison of a bio-based corrosion inhibitor versus benzatriazole on corroded copper surfaces, Corros. Sci. 143 (2018) 84-92, https://doi.org/10.1016/j.corsci.2018.08.020

[8] L. Robbiola, C. Fiaud, S. Pennec, New model of outdoor bronze corrosion and its implications for conservation, ICOM committee for conservation (1993) 796-802, https://hal.archives-ouvertes.fr/hal-00975704

[9] D.A. Scott, Bronze disease: A review of some chemical problems and the role of relative humidity, J. of the American Institute for Conservation 29 (1990) 193-206, https://doi.org/10.1179/019713690806046064

[10] D.A. Scott, A review of copper chlorides and related salts in bronze corrosion and as painting pigments, Studies in conservation 45 (2000) 39-53, https://doi.org/10.1179/sic.2000.45.1.39

[11] X. Zhang, I. O. Wallinder, C. Leygraf, Mechanistic studies of corrosion product flaking on copper and copper-based alloys in marine environments, Corros. Sci. 85 (2014) 15-25, https://doi.org/10.1016/j.corsci.2014.03.028

[12] I. O. Wallinder, X. Zhang, S. Goidanich, N. Le Bozec, G. Herting, C. Leygraf, Corrosion and runoff rates of Cu and three Cu-alloys in marine environments with increasing chloride deposition rate, Sci. Total Environ. 472 (2014) 681-694, https://doi.org/10.1016/j.scitotenv.2013.11.080

[13] T. Chang, G. Herting, S. Goidanich, J.M. Sánchez Amaya, M.A. Arenas, N. Le Bozec, Y. Jin, C. Leygraf, I. O Wallinder The role of Sn on the long-term atmospheric corrosion of binary Cu-Sn bronze alloys in architecture, Corros. Sci. 149 (2019) 54-67, https://doi.org/10.1016/j.corsci.2019.01.002

[14] T. Chang, A. Maltseva, P. Volovitch, I. O Wallinder, C. Leygraf, A mechanistic study of stratified patina evolution on Sn-bronze in chloride rich atmospheres, Corros. Sci. 166 (2020) 108477, https://doi.org/10.1016/j.corsci.2020.108477

[15] N.D. Meeks, Patination phenomena on Roman and Chinese high-tin bronze mirrors and other artefacts, in S. La Niece, P. Craddock (Eds), Metal Plating and Patination Cultural, Technical and Historical Developments (1993) 63-84, https://doi.org/10.1016/B978-0-7506-1611-9.50010-8

[16] W.T. Chase, Chinese bronzes: casting, finishing, patination and corrosion, in:D.A. Scott, J. Podany, B. Considine (Eds.), Ancient, Historic Metals, The Getty Conservation Institute, London (1994) 85-117

[17] M. De Bondt, A. Deruyttere, Pearlite and bainite formation in a cu-16.5 at.% sn alloy, Acta Met. 15 (1967) 993-1005, https://doi.org/10.1016/0001-6160(67)90264-7

[18] Z. Shoukang, H. Tangkun, Studies of ancient Chinese mirrors and other bronze artefacts, in S. La Niece, P. Craddock (Eds), Metal Plating and Patination Cultural, Technical and Historical Developments (1993) 50-62, https://doi.org/10.1016/B978-0-7506-1611-9.50009-1

[19] D.A. Scott, Metallography and Microstructure of Ancient and Historic Metals, Getty Conservation Institute Publications, Los Angeles, (1991)

[20] A.G. Nord, K. Tronner, A.J. Boyce, Atmospheric bronze and copper corrosion as an environmental indicator. A Study Based on Chemical and Sulphur Isotope Data, Water, Air, Soil Pollut. 127 (2001) 193-204, https://doi.org/10.1023/A:1005254913598

[21] C. Chiavari, E. Bernardi, C. Martini, F. Passarini, F. Ospitali, L. Robbiola, The atmospheric corrosion of quaternary bronzes: The action of stagnant rain water, Corros. Sci. 52 (2010) 3002-3010, https://doi.org/doi:10.1016/j.corsci.2010.05.013

[22] D.J. Chakrabarti, D.E. Laughlin, The Cu–Pb (Copper-Lead) system, Bull. Alloy Phase Diagr. 5 (1984) 503-510, https://doi.org/10.1007/BF02872905

[23] K. Kareem, S. Sultan, L. He, Fabrication, microstructure and corrosive behavior of different metallographic tin-lead bronze alloys part II: Chemical corrosive behavior and patina of tin-leaded bronze alloys, Mater. Chem. Phys. 169 (2016) 158-172, https://doi.org/10.1016/j.matchemphys.2015.11.044

[24] R. L. Frost, W. Martens, J.T. Kloprogge, Z. Ding, Raman spectroscopy of selected lead minerals of environmental significance, Spectrochim. Acta Part A 59 (2003) 2705-2711, https://doi.org/10.1016/S1386-1425(03)00054-4

[25] E. B. Melchiorre, H. A. Gilg, Oxygen stable isotope fractionation behavior of cerussite and hydrocerussite: New results and reconciliation of the recent literature, Geochim. Cosmochim. Acta, 75 (2011) 3191-3195, https://doi.org/10.1016/j.gca.2011.03.013

[26] D. Dermatas, M. Dadachov, P. Dutko, N. Menounou, P. Arienti, G. Shen, Weathering of lead in fort irwin firing range soils, Global Nest : the Int. J. 6 (2004) 171-179, https://doi.org/10.30955/gnj.000251

[27] H. Liu, G. V. Korshin, J. F. Ferguson, Investigation of the Kinetics and Mechanisms of the Oxidation of Cerussite and Hydrocerussite by Chlorine, Environ. Sci. Technol. 42 (2008) 3241-3247, https://doi.org/10.1021/es7024406

[28] E. Bernardi, C. Chiavari, C. Martini, L. Morselli, The atmospheric corrosion of quaternary bronzes: An evaluation of the dissolution rate of the alloying elements, Appl. Phys. A 92 (2008) 83-89, https://doi.org/10.1007/s00339-008-4451-0

[29] Y. Zhang, Y.-P. Lin, Adsorption of Free Chlorine on Tetravalent Lead Corrosion Product (PbO_2), Environ. Eng. Sci. 29 (2012) 52-58, https://doi.org/10.1089/ees.2010.0372

[30] R.L. Frost, Raman spectroscopy of selected copper minerals of significance in corrosion, Spectrochim. Acta Part A 59 (2003) 1195-1204, https://doi.org/10.1016/S1386-1425(02)00315-3

[31] J.B. Launay, Manuel du fondeur sur tous métaux, ou Traité de toutes les opérations de la fonderie, Roret – Paris (Ed) tome 1 (1827) 274-304, https://gallica.bnf.fr/ark:/12148/bpt6k62000p.texteImage

[32] J. Audy, K. Audy, Effects of microstructure and chemical composition on strength and impact toughness of tin bronze, MM Science Journal (2009) 125-130, https://doi.org/10.17973/MMSJ.2009_06_20090303

[33] C.P. Swann, S.J. Fleming, M. Jaksic, Recent applications of PIXE spectrometry in archeology: I. characterization of bronzes with special consideration of the influence of corrosion processes on data reliability, Nucl. Instrum. Meth. B 64 (1992) 499-504, https://doi.org/10.1016/0168-583X(92)95523-T

[34] R.J.C. Silvia, E. Figueiredo, M.F. Araújo, F. Pareira, F.M. Braz Fernandes, Microstructure interpretation of copper and bronze archeological artefacts from Portugal,

Mater. Sci. Forum 587-588 (2008) 365-369, https://doi.org/10.4028/www.scientific.net/MSF.587-588.365

[35] V. Debut, M. Carvalho, E. Figueiredo, J. Antunes, R. Silva, The sound of bronze: Virtual resurrection of a broken medieval bell, J. Cult. Herit., 19 (2016) 544-554, https://doi.org/10.1016/j.culher.2015.09.007

[36] A. Vazdirvanidis, G. Pantazopoulos, Metallographic Study of Great Anthony Historical Bronze Bells of Apostle Andrew Skete in Mount Athos, Greece Metallogr. Microstruct. Anal. 6 (2017) 340-351, https://doi.org/10.1007/s13632-017-0363-8

[37] M. Goodway, V. C. Pigott, High-tin bronze gong making, part I of two, J. Metals 40 (1988) 36-37, https://vdocuments.net/download/ancient-metal-mirror-making-in-south-india https://doi.org/10.1007/BF03258939

[38] M. Goodway, V. C. Pigott, High-tin bronze gong making, part II of two, J. Metals 40 (1988) 62-63, https://doi.org/10.1007/BF03259026

[39] J.S. Park, R. B. Gordon, Traditions and transitions in Korean bronze technology, J.A.S. 34 (2007) 1991-2002, https://doi.org/10.1016/j.jas.2007.01.010

[40] M. Taube, A. H. King, W.T. Chase, Transformation of ancient Chinese and model two-phase bronze surfaces to smooth adherent patinas, Phase Transitions, 81 (2008) 217-232 https://doi.org/10.1080/01411590701514375

[41] W.T. Chase, U.M. Franklin, Early Chinese black mirrors and pattern-etched weapons. Ars Orientalis, 11 (1979) 215-258, https://www.jstor.org/stable/4629305

[42] L. Robbiola, PhD Thesis, Sorbonne University-Campus of Pierre et Marie Curie, France (1990), https://tel.archives-ouvertes.fr/tel-00495356/fr

[43] D.A. Scott, Periodic corrosion phenomena in Bronze antiquities, Stud. Conserv. 30 (1985) 49-57, https://doi.org/10.2307/1506088

[44] G.M. Ingo, T. de Caro, C. Riccucci, E. Angelini, S. Grassini, S. Balbi, P. Bernardini, D. Salvi, L. Bousselmi, A. Çilingiroglu, M. Gener, V.K. Gouda, O. Al Jarrah, S. Khosroff, Z. Mahdjoub, Z. Al Saad, W. El-Saddik, P. Vassiliou, Large scale investigation of chemical composition, structure and corrosion mechanism of bronze archaeological artefacts from Mediterranean basin, Appl. Phys. A 83 (2006) 513-520, https://doi.org/10.1007/s00339-006-3550-z

[45] G.M.Ingo, C.Riccucci, C.Giuliani, A.Faustoferri, I.Pierigè, G.Fierro, M.Pascucci, M.Albini, G.Di Carlo, Surface studies of patinas and metallurgical features of uncommon high-tin bronze artefacts from the Italic necropolises of ancient Abruzzo (Central Italy), Appl. Surf. Sci. 470 (2019) 74-83, https://doi.org/10.1016/j.apsusc.2018.11.115

[46] C. Bosi, G. L. Garagnani, V. Imbeni, C. Martini, R. Mazzeo, G. Poli, Unalloyed copper inclusions in ancient bronze artefacts, J. Mater. Sci. 37 (2002) 4285-4298, https://doi.org/10.1023/A:1020640216415

[47] Q. Wang, J. F. Merkel, Studies on the Redeposition of Copper in Jin Bronzes from Tianma-Qucun, Shanxi, China, Stud. Conserv., 46, (2001) 242-250, https://doi.org/10.2307/1506774

[48] H. Wei, W. Kockelmann, E. Godfrey, D. A. Scott, The metallography and corrosion of an ancient chinese bimetallic bronze sword, J. Cult. Herit., 37 (2019) 259-265, https://doi.org/10.1016/j.culher.2018.10.004

[49] T.H. Randle, Galvanic corrosion - A kinetic study. J. Chem. Educ. 71 (1994) 261–265, https://doi.org/10.1021/ed071p261

[50] C. Cartier, R.B. Arnold, S. Triantafyllidou, M. Prévost, M. Edwards, Effect of flow rate and Lead/Copper pipe sequence on lead release from service lines. Water Res. 46 (2012) 4142–4152, https://doi.org/10.1016/j.watres.2012.05.010

[51] C.K. Nguyen, K.R. Stone, M.A. Edwards, Chloride-to-sulfate mass ratio: practical studies in galvanic corrosion of lead solder, J. Am. Water Work. Assoc. 103 (2011) 81-92, https://doi.org/10.1002/j.1551-8833.2011.tb11384.x

[52] Y. Wang, H.Jing, V. Mehta, G.J. Welter, D.E. Giammar, Impact of galvanic corrosion on lead release from aged lead service lines, Water Res. 46 (2012) 5049-5060, https://doi.org/10.1016/j.watres.2012.06.046.

[53] D. Q. Ng, Y.P. Lin, Effects of pH value, chloride and sulfate concentrations on galvanic corrosion between lead and copper in drinking water, Environ. Chem. 13 (2016) 602-610, https://doi.org/10.1071/EN15156

[54] C.S. Smith, A search for structure, MIT Press Ed, Cambridge, Mass. USA, (1981) 85-88.

[55] J. Muller, B. Laïk, I. Guillot, α-CuSn bronzes in sulphate medium: influence of the tin content on corrosion processes, Corros. Sci. 77 (2013) 46-51, https://doi.org/10.1016/j.corsci.2013.07.025

[56] W.M. Haynes ed., Thermochemistry, electrochemistry and solution chemistry, in CRC Handbook of Chemistry and Physics, 97th Edition 2016-2017, 5-11,5-39

[57] H. Strandberg, L.G. Johansson, Some Aspects of the Atmospheric Corrosion of Copper in the Presence of Sodium Chloride, J. Electrochem. Soc., 145 (1998) 1093-1100, https://doi.org/10.1149/1.1838422

Aggressiveness of marine environment

Shocks and vibrations on brittle corrosion products

✓clapper or hammer impacts

✓fixation point of the crown

+

Micro-structure of the bronze bell

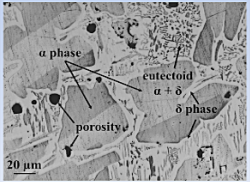

Micro-infiltrating corrosion

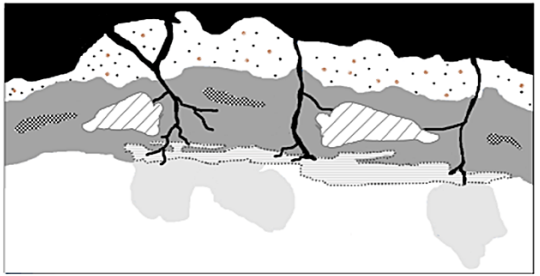

External layer- Transformed medium

Quartz / Iron

Intermediate layer

α/δ Internal corrosion pitting

Joining of corrosion pitting

Conductive corrosion products

Cracks

Alloy

Alloy fragments rich in tin oxide (Type I corrosion)